HEFAT2012
9th International Conference on Heat Transfer, Fluid Mechanics and Thermodynamics
16 – 18 July 2012
Malta

EMPIRICAL CORRELATIONS FOR GRID TURBULENCE

Lee S.K.*, Djenidi L, and Antonia R.A.
*Author for correspondence
School of Engineering,
The University of Newcastle,
NSW, 2308,
Australia,
E-mail: soon-kong.lee@newcastle.edu.au

ABSTRACT

Homogeneous isotropic turbulence (HIT) is approximately generated by passing a uniform flow through a grid followed by a short contraction. The grid flow is slightly heated so that temperature acts as a passive scalar. In the self-similar region of grid flow downstream of the contraction, there is no mean shear and no turbulence production. The amplitudes of velocity and temperature fluctuations simply decay under the effect of viscosity and thermal diffusion. The decay rate is well represented by a power law; this is supported by present measurements in three different grid flows and by previously published data for grid turbulence obtained over different ranges of streamwise distance and/or Reynolds number. From dimensional analysis and the (empirical) power-law correlations, basic flow parameters, namely the Kolmogorov/Taylor/ Corrsin microscales and the Reynolds/Péclet numbers, are established as functions of streamwise distance. From this, it is possible to determine the flow parameters for a required grid geometry or initial condition.

INTRODUCTION

In turbulent mixing, the kinetic energy cascaded down from larger to smaller eddies is removed at the smallest scales by viscous dissipation. The energy flux across the different scales is a measure of the dissipation rate. The mean dissipation rate is important because it determines the characteristic length scales in grid turbulence. Grid turbulence [e.g. 1-4] is of particular interest because it closely approximates the least complex form of turbulence, i.e. HIT. The similarity analysis of this flow enables one to test the concept of universal behaviour of turbulence. Since grid turbulence is usually tested in wind tunnels, it is useful and often necessary to first determine that the basic flow parameters can be met for a particular facility prior to carrying out an experiment.

In the flow under consideration (i.e. HIT), the free-stream velocity is uniform and the variance of streamwise fluctuation $< u^2 >$ is equal to the variance of cross-stream fluctuations

NOMENCLATURE

d	[m]	Diameter or width of grid bar
d_{cold}, d_{hot}	[m]	Diameter of cold/hot wire
f_K	[Hz]	Kolmogorov frequency
l_{cold}, l_{hot}	[m]	Length of cold/hot wire
M	[m]	Mesh size of grid
n_u, n_q	[-]	Power-law decay rate(s) of velocity fluctuation
n_θ	[-]	Power-law decay rate of scalar fluctuation
Pe	[-]	Péclet number
Pr	[-]	Prandtl number
$< q^2 >$	[m^2/s^2]	Mean turbulence kinetic energy
r_*	[-]	Anisotropy ratio of grid turbulence
R	[-]	Ratio between scalar and velocity timescales
R_M	[-]	Grid mesh Reynolds number
R_λ	[-]	Taylor microscale Reynolds number
$t = x/U_o$	[s]	Time for turbulence to be convected from grid
t_o, t_o^u, t_o^θ	[s]	Virtual origin of turbulence/scalar fluctuation
$< u^2 >$	[m^2/s^2]	Streamwise velocity fluctuation
U_{cl}	[m/s]	Centerline velocity in test section
U_o	[m/s]	Free stream velocity entering the grid
$< v^2 >$, $< w^2 >$	[m^2/s^2]	Cross-stream velocity fluctuations
x	[m]	Streamwise distance from the grid

Special characters

α_u, α_θ	[-]	Amplitude of velocity/scalar fluctuation
$< \chi >$	[^{o}C^2/s]	Mean dissipation rate of scalar variance
$< \varepsilon >$	[m^2/s^3]	Mean dissipation rate of turbulence energy
η	[m]	Kolmogorov length scale
λ, λ_θ	[m]	Taylor/Corrsin (thermal) microscale
κ	[m^2/s]	Thermal diffusivity
ν	[m^2/s]	Kinematic viscosity
σ	[-]	Solidity ratio of the grid mesh
τ, τ_θ	[s]	Timescale of velocity/scalar fluctuation
$< \theta^2 >$	[^{o}C]	Passive scalar (temperature) fluctuation
ΔT	[^{o}C]	Difference between grid flow temperature and ambient air temperature

$< v^2 >$ and $< w^2 >$ (the angular brackets denote time-averaged value). The mean turbulence energy is written as

$$< q^2 > = < u^2 > + < v^2 > + < w^2 > = \left(1+\frac{2}{r_*}\right) < u^2 >, \quad (1)$$

and the mean energy dissipation rate is defined as

$$< \varepsilon > = -\frac{1}{2}\frac{d < q^2 >}{dt} = -\frac{1}{2}\left(1+\frac{2}{r_*}\right)\frac{d < u^2 >}{dt}, \quad (2)$$

where $r_* = < u^2 > / < v^2 > = < u^2 > / < w^2 >$ serves as a measure of large-scale isotropy. Studies [1-3] have shown that, by stretching the grid flow with a contraction (area ratios of 1.27 and 1.36) downstream of a grid, the anisotropy ratio may be reduced from $1.1 \le r_* \le 1.8$ down to $0.9 \le r_* \le 1.2$. Notably, with a $1.36:1$ contraction, and for a round-bar grid of 44% solidity with a wire helically wrapped around each bar, measurements [2, 3] have shown that $r_* \approx 0.99$; we shall refer to this grid, known as "Rd44w", in later sections of this paper.

It is well established [1-3, 5, 6] that, in the self-similar region of flow downstream of the initially developing grid turbulence and/or accelerated decay due to the contraction, both $< q^2 >$ and $< \varepsilon >$ exhibit a power-law rate of decay, i.e.

$$< q^2 > = \left(1+\frac{2}{r_*}\right)\alpha_u \left(t - t_o^u\right)^{n_u} \quad (3)$$

$$< \varepsilon > = -\frac{1}{2}\left(1+\frac{2}{r_*}\right)\alpha_u n_u \left(t - t_o^u\right)^{n_u - 1}, \quad (4)$$

where α_u and t_o^u depend on initial conditions. In HIT, the decay rates for both $< u^2 >$ and $< q^2 >$ should be the same, i.e. $n_u = n_q < 0$. When a scalar, such as temperature θ, is introduced in the flow so that it does not affect the dynamics of the flow (i.e. it is "passive"), both the scalar variance $< \theta^2 >$ and the mean scalar dissipation rate $< \chi >$ also exhibit a power-law rate of decay [6-9], i.e.

$$< \theta^2 > = \alpha_\theta \left(t - t_o^\theta\right)^{n_\theta}, \quad (5)$$

$$< \chi > = -\frac{1}{2}\frac{d < \theta^2 >}{dt} = -\frac{1}{2}\alpha_\theta n_\theta \left(t - t_o^\theta\right)^{n_\theta - 1}, \quad (6)$$

where α_θ, t_o^θ and $n_\theta < 0$ depend on how the passive scalar is introduced in the flow.

From (1)-(6), it is possible to define certain characteristic scales in grid turbulence. For this paper, our interest is on the Kolmogorov length scale and the Taylor/Corrsin microscales (defined in the next section). Dimensional analysis is used to show how these scales can be related to Reynolds number and streamwise distance from the grid. In this study, we present simultaneous measurements of velocity and temperature in grid turbulence at small Reynolds numbers. The results, supplemented with previously published data for grid turbulence obtained at large Reynolds numbers [10] and/or at large downstream distances from the grid [1, 11], should be useful for providing information on the basic flow parameters for scaling grid turbulence in general.

CHARACTERISTIC SCALES

The Kolmogorov length scale (η) is a measure of the smaller eddies affected by viscous dissipation. It is defined as

$$\eta = \frac{\nu^{3/4}}{< \varepsilon >^{1/4}}, \quad (7)$$

where ν is the kinematic viscosity of the fluid. For the Taylor and Corrsin microscales, they apply to larger eddy sizes; the velocity and scalar (thermal) spectra non-dimensionalised by the respective Taylor and Corrsin microscales provide a reasonable collapse over a wide range of wavenumbers [7]. The isotropic forms of the Taylor microscale (λ) and the Corrsin (thermal) microscale (λ_θ) are written as [7, 12, 13]

$$\lambda = \left(\frac{< u^2 >}{< (\partial u/\partial x)^2 >}\right)^{1/2} = \left(\frac{5\nu < q^2 >}{< \varepsilon >}\right)^{1/2}; \quad (8)$$

$$\lambda_\theta = \left(\frac{2 < \theta^2 >}{< (\partial \theta/\partial x)^2 >}\right)^{1/2} = \left(\frac{6\kappa < \theta^2 >}{< \chi >}\right)^{1/2}, \quad (9)$$

which, by observing the power laws (3)-(6), may be recast as

$$\lambda = \left[-\frac{10\nu}{n_u}\left(t - t_o^u\right)\right]^{1/2}; \quad (10)$$

$$\lambda_\theta = \left[-\frac{12\kappa}{n_\theta}\left(t - t_o^\theta\right)\right]^{1/2}, \quad (11)$$

where κ is the thermal diffusivity of the fluid. From the relations (8)-(11), we obtain the Taylor/Corrsin-microscale ratio

$$\frac{\lambda}{\lambda_\theta} = \left(\frac{5}{6}\frac{Pr}{R}\right)^{1/2}, \quad (12)$$

where $Pr = \nu/\kappa$ is the Prandtl number, and

$$R = \frac{\tau_\theta}{\tau} = \frac{< \theta^2 > / < \chi >}{< q^2 > / < \varepsilon >} \quad (13)$$

is the scalar/velocity timescale ratio. Usually, in HIT, and for a passive scalar introduced just downstream of the grid, the decay rates for both $< q^2 >$ and $< \theta^2 >$ should be nearly about the same, i.e. $R \approx n_u / n_\theta \approx 1$.

Two different velocity scales are used to characterise grid turbulence. They are the Taylor microscale Reynolds number

$$R_\lambda = \frac{\lambda\left(< q^2 > /3\right)^{1/2}}{\nu}, \quad (14)$$

and the grid mesh Reynolds number

$$R_M = \frac{M U_o}{\nu}, \quad (15)$$

where M is the mesh size of the grid, and U_o is the free-stream (or mean) velocity entering the grid. Relations (14) and (15) represent the effects of viscosity on the grid flow. To

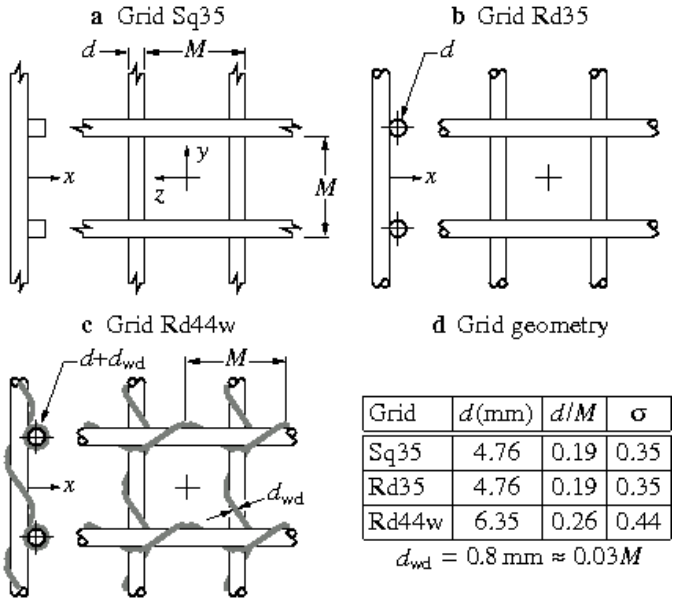

Grid	d(mm)	d/M	σ
Sq35	4.76	0.19	0.35
Rd35	4.76	0.19	0.35
Rd44w	6.35	0.26	0.44

$d_{wd} = 0.8\,\text{mm} \approx 0.03M$

Figure 1 Geometry of the biplanar grids; the mesh solidity is $\sigma = d/M\left(2-d/M\right)$; x axis is on the centerline of the duct

describe the effect of thermal diffusion in grid turbulence, we define the molecular Péclet number

$$Pe = \frac{\lambda_\theta \left(< q^2 > /3\right)^{1/2}}{\kappa}, \qquad (16)$$

which simplifies to $Pe = \left(\nu/\kappa\right) R_\lambda$ if $\lambda/\lambda_\theta = 1$.

The following section begins by describing the technique used to measure grid turbulence in a wind tunnel.

EXPERIMENTAL METHOD

Figure 1 shows the three different grids used for this study. The first grid (Sq35) is made of square bars with a solidity ratio (σ) of 0.35, the second grid (Rd35) has round bars ($\sigma = 0.35$) and the third grid (Rd44w) consists of round bars with a fine wire wrapped around each bar ($\sigma = 0.44$). For each grid, the size of the mesh is $M = 24.76$ mm. Figure 2 shows examples of large-scale structures produced behind a biplanar grid (in water); these structures generally persist for a short distance downstream of the grid and they rapidly become indiscernible in the self-similar region of flow downstream of the initially developing turbulence (i.e. $> 20M$) [2].

The present experiments are performed using the same open-circuit wind tunnel as that described by Lavoie [2] and Lavoie *et al*. [3]. The test section (Figure 3) includes a short 1.36:1 secondary contraction (located at $11M$ downstream of the grid) for the purpose of improving isotropy at the large scales. The design of the contraction is based on a linear theory of turbulence [14, 15] and the empirical data of Comte-Bellot and Corrsin [1]. Given that the velocity through the contraction is not constant, the time for turbulence to be convected from the grid (at location $s = 0$) to a downstream

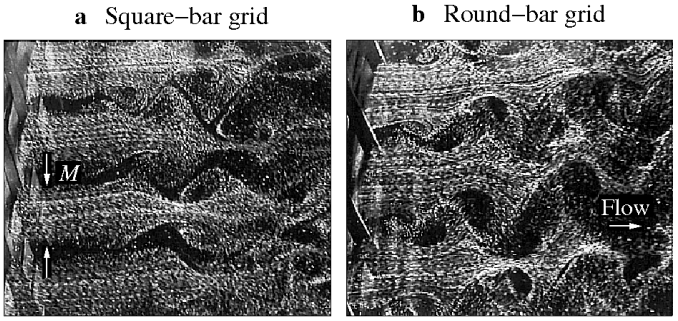

Figure 2 Hydrogen bubble visualisation of Lavoie [2] showing typical large-scale structures just downstream of the grid.

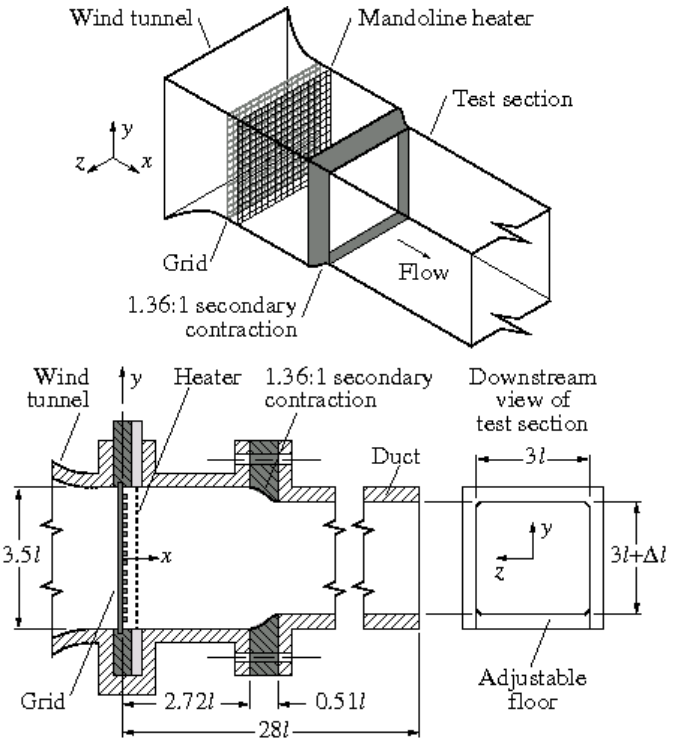

Figure 3 Wind-tunnel test section. Scale: $l = 0.1\text{m} \simeq 0.4M$

position ($s = x$) is defined by [1-4]

$$t = \int_0^x \frac{ds}{< U(s) >}. \qquad (17)$$

The dimensionless time scale tU_o/M is used to allow direct comparison between grid-flow results obtained downstream of the secondary contraction and those obtained without a contraction. With no contraction, (17) simplifies to $t = x/U_o$. The free-stream (or mean) velocity U_o is the centerline velocity $U_{cl}(x)$ of the wind-tunnel flow in the absence of a grid; the measurements of $U_{cl}(x)$ in Figure 4 are obtained using a Pitot-static probe and a (100-Pa) micro-manometer. The variation in wall pressure over the region of constant velocity ($18 < x/M < 100$) is $\leq 1\%$ of the dynamic pressure.

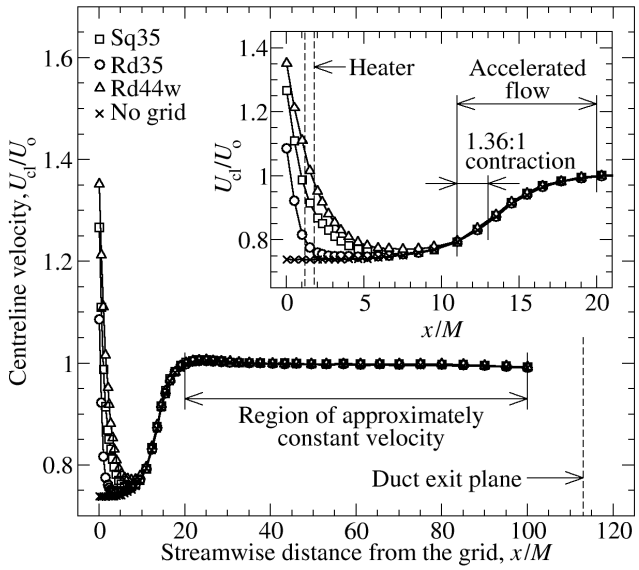

Figure 4 Distribution of centerline velocity in the test section

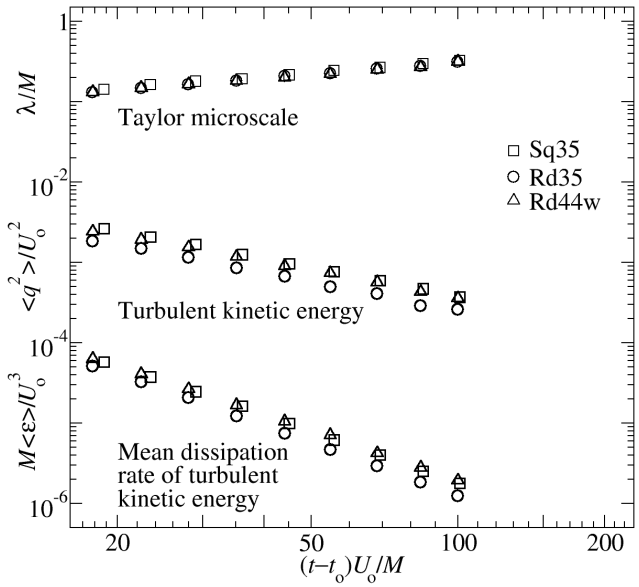

Figure 5 Mean turbulent kinetic energy, mean energy dissipation rate, and the Taylor microscale for the different grids

The flow is heated with a mesh of 0.5-mm-diameter Chromel-A wires placed at $1.5M$ downstream of the grid (Figure 3); the wires are too fine to shed vortices and thus affect the velocity field. The horizontal and vertical wires of the heater are separated by a gap of $0.6M$ and have the same mesh size as the grids. The temperature is controlled by a variable-voltage ($0 \rightarrow 275\mathrm{V}$) power supply. This method of heating is the same as that described by Zhou *et al.* [9]. For the temperature to be passive, the grid flow is slightly warmer than the ambient air (the temperature difference is $\Delta T \approx 2^{\circ}\mathrm{C}$).

The fluctuations in velocity (streamwise component u) and temperature (θ) are measured simultaneously using hot and cold (Wollaston Pt-10%Rh) wires. The hot wire (diameter $d_{\mathrm{hot}} \approx 2.50\mu\mathrm{m}$; length $l_{\mathrm{hot}} \approx 200 d_{\mathrm{hot}}$) is operated at constant temperature (the overheat ratio is 1.5) and the cold wire ($d_{\mathrm{cold}} \approx 0.63\mu\mathrm{m}$; $l_{\mathrm{cold}} \approx 1000 d_{\mathrm{cold}}$) is operated at a constant current of $0.1\mathrm{mA}$ (the sensitivity is $1\Omega/^{\circ}\mathrm{C}$). The wires are parallel with a spanwise separation of $1\mathrm{mm}$ and the cold wire is located just slightly upstream of the hot wire. The spacing between the wires is 1.5-3.0η. The wire lengths, from the measurement position nearest to the grid to that furthest from the grid, are $0.6 \le \eta/l_{\mathrm{hot}} < 1.5$ and $0.5 < \eta/l_{\mathrm{cold}} \le 1.1$.

The hot and cold wire signals are digitised with a 12bit A/D converter and are low-pass filtered at half the sampling rate. The cutoff frequency of the filter is determined by the response time of the cold wire [16]; it is usually just smaller than the Kolmogorov frequency, i.e. $0.8 \le f_{\mathrm{K}}(2\pi\eta/U_{\mathrm{o}}) < 1$. For each measurement point, the sampling period is $t_s U_o/\eta \approx 10^6$; η varies with streamwise distance from the gird; the sample size is one million. The Reynolds and Prandtl numbers are $R_M \simeq 10^4$ and $Pr \simeq 0.71$ respectively.

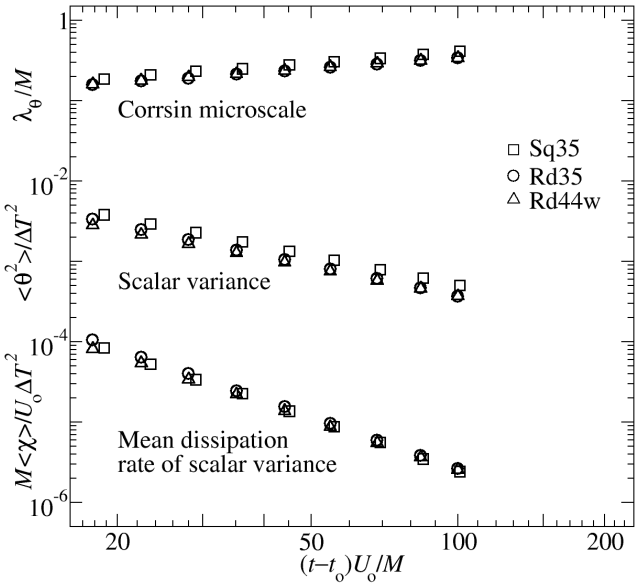

Figure 6 Temperature variance, mean scalar dissipation rate, and the Corrsin microscale for the different grids

RESULTS AND DISCUSSION

The present measurements are shown in Figures 5 to 7. Lavoie *et al.* [3] measured $r_* = <u^2>/<w^2>$ in the central core region of the same grid flows. We have used the axial symmetry of the flows to estimate $<q^2>$, i.e. Equation (1), using the present measurements of $<u^2>$. For each grid, $<q^2>$, $<\varepsilon>$, λ, $<\theta^2>$, $<\chi>$ and λ_θ undergo changes

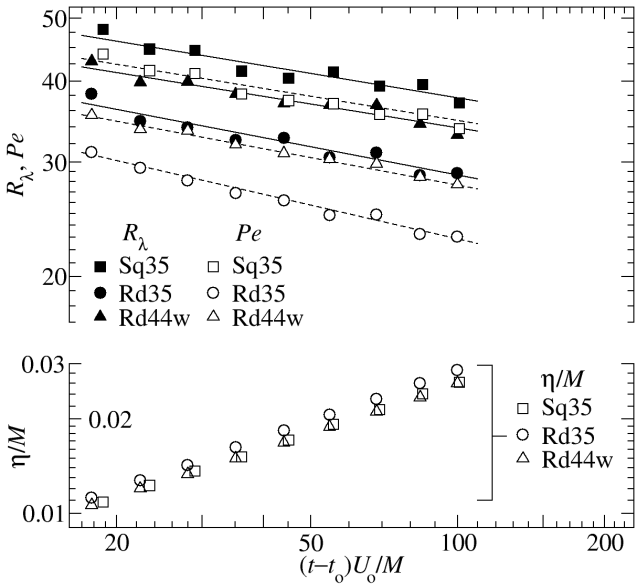

Figure 7 Taylor microscale Reynolds number, Péclet number and the Kolmogorov microscale for the different grids

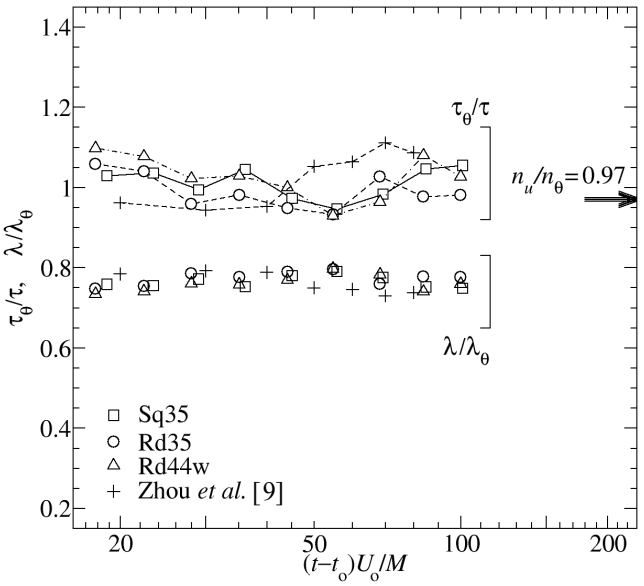

Figure 8 Scalar/velocity time-scale ratio for the different grids

and the resulting values of R_λ and Pe also changes. Note that the different grids, as felt by the large scales through $<q^2>$, affects R_λ and Pe more than η. From dimensional analysis, we readily obtain the following functions for the flow parameters η, λ, λ_θ, R_λ and Pe:

$$\frac{\eta}{M} = \mathrm{f}_1\left(R_M, \frac{M<\varepsilon>}{U_o^3}\right), \tag{18}$$

$$\frac{\lambda}{M} = \mathrm{f}_2\left(R_M, \frac{<q^2>}{U_o^2}, \frac{M<\varepsilon>}{U_o^3}\right), \tag{19}$$

$$\frac{\lambda_\theta}{M} = \mathrm{f}_3\left(R_M, Pr, \frac{<\theta^2>}{\Delta T^2}, \frac{M<\chi>}{U_o\Delta T^2}\right), \tag{20}$$

$$R_\lambda = \mathrm{f}_4\left(R_M, \frac{<q^2>}{U_o^2}, \frac{M<\varepsilon>}{U_o^3}\right) \tag{21}$$

and

$$Pe = \mathrm{f}_5\left(R_M, Pr, \frac{<q^2>}{U_o^2}, \frac{<\theta^2>}{\Delta T^2}, \frac{M<\chi>}{U_o\Delta T^2}\right). \tag{22}$$

The normalisation uses M, U_o and ΔT. By using (7)-(9) and (14)-(16), we obtain the following dimensionless groups:

$$\frac{\eta}{M} R_M^{3/4} = \left(\frac{M<\varepsilon>}{U_o^3}\right)^{-1/4}, \tag{23}$$

$$\frac{\lambda}{M} R_M^{1/2} = \left(\frac{5<q^2>/U_o^2}{M<\varepsilon>/U_o^3}\right)^{1/2}, \tag{24}$$

$$\frac{\lambda_\theta}{M}\left(R_M Pr\right)^{1/2} = \left[\frac{6<\theta^2>/\Delta T^2}{M<\chi>/\left(U_o\Delta T^2\right)}\right]^{1/2}, \tag{25}$$

$$\frac{R_\lambda}{R_M^{1/2}} = \frac{<q^2>/U_o^2}{\left[(3/5)\left(M<\varepsilon>/U_o^3\right)\right]^{1/2}} \tag{26}$$

and

$$\frac{Pe}{\left(R_M Pr\right)^{1/2}} = \left[\frac{2\left(<q^2>/U_o^2\right)\left(<\theta^2>/\Delta T^2\right)}{M<\chi>/\left(U_o\Delta T^2\right)}\right]^{1/2}. \tag{27}$$

Given that the trends in Figures 5 and 6 reasonably follow power laws of the forms (3)-(6), i.e. one could draw a straight line through each set of the data points, it is possible to recast the dimensionless groups (23)-(27) as

$$\frac{\eta}{M} R_M^{3/4} = \left[-\frac{1}{2}\left(1+\frac{2}{r_*}\right)\alpha_u n_u\right]^{-1/4}\left[\frac{\left(t-t_o\right)U_o}{M}\right]^{(1-n_u)/4}, \tag{28}$$

$$\frac{\lambda}{M} R_M^{1/2} = \left[-\frac{10}{n_u}\frac{\left(t-t_o\right)U_o}{M}\right]^{1/2}, \tag{29}$$

$$\frac{\lambda_\theta}{M}\left(R_M Pr\right)^{1/2} = \left[-\frac{12}{n_\theta}\frac{\left(t-t_o\right)U_o}{M}\right]^{1/2}, \tag{30}$$

$$\frac{R_\lambda}{R_M^{1/2}} = \left[-\frac{10}{3}\frac{\alpha_u}{n_u}\left(1+\frac{2}{r_*}\right)\right]^{1/2}\left[\frac{\left(t-t_o\right)U_o}{M}\right]^{(1+n_u)/2} \tag{31}$$

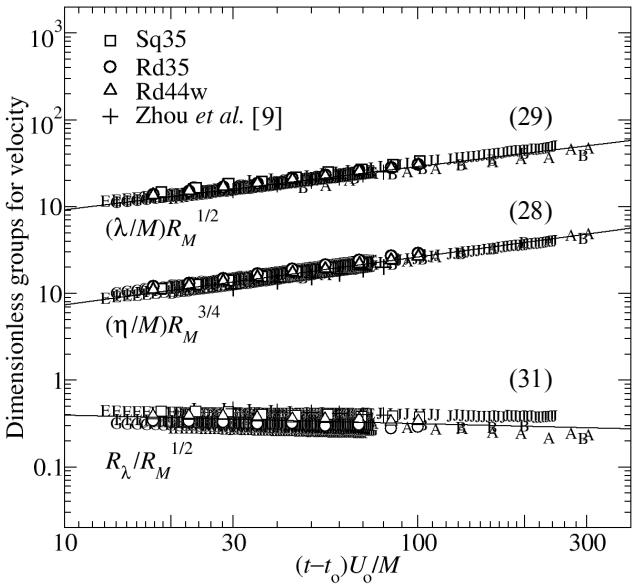

Figure 9 Velocity in grid turbulence; (A), (B) Comte-Bellot and Corrsin [1]; (C) Kistler and Verbalovich [9]; (D)-(I) Lavoie [2] and Lavoie *et al.* [3]; (J) Krogstad and Davidson [10]; the other symbols are defined in the legend. The empirical correlations are for $r_* = 1.0$, $\alpha_u = 0.03$ and $n_u = -1.20$. The top set of data points are vertically offset by a factor of 10

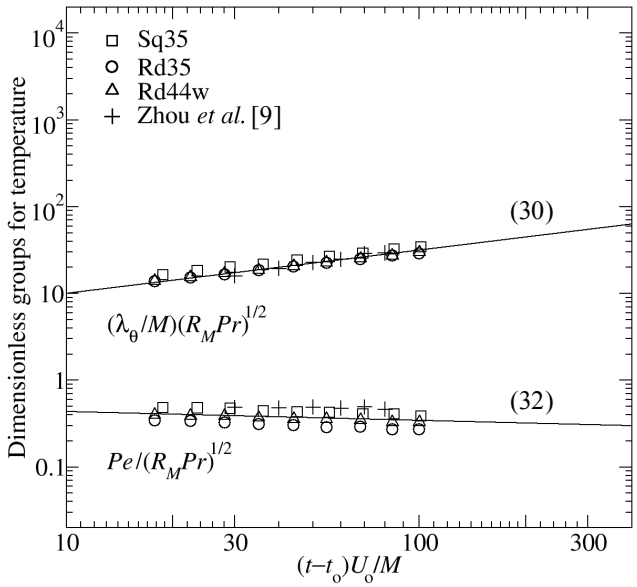

Figure 10 Passive scalar (temperature) in grid turbulence; the correlations are for $r_* = 1.0$, $\alpha_u = 0.03$ and $n_u = n_\theta = -1.20$

and

$$\frac{Pe}{\left(R_M Pr\right)^{1/2}} = \left[-4\frac{\alpha_u}{n_\theta}\left(1+\frac{2}{r_*}\right)\right]^{1/2}\left[\frac{\left(t-t_o\right)U_o}{M}\right]^{(1+n_u)/2}, \tag{32}$$

where t_o, r_*, α_u, n_u and n_θ are the empirical coefficients. For the present measurements, the virtual origin t_o is determined via the Taylor/Corrsin microscales given by (10) and (11); this method of determining t_o is described elsewhere [2, 3, 6]. For each grid (Figures 5 to 7), the same optimum value of virtual origin satisfies both the velocity and the temperature measurements (i.e. $t_o = t_o^u \simeq t_o^\theta$); changing $t_o U_o/M$ by ± 1.0 alters n_u and n_θ by not more than ± 0.03. For all three present grids, the ratio n_u/n_θ is 0.97; the values of n_u are -1.18 (Sq35), -1.23 (Rd35) and -1.14 (Rd44w). As shown in Figure 8, we have checked that the timescale ratio τ_θ/τ indeed closely matches the ratio n_u/n_θ. The ratios τ_θ/τ and λ/λ_θ are reasonably independent of tU_o/M although the larger variations observed in τ_θ/τ suggest that this parameter is sensitive to the large scales (Figure 8). For the present data, the uncertainty in estimating τ_θ/τ using (13), reflected by the uncertainty in the measurements of $<\varepsilon>$ and $<\chi>$, is $\pm 10\%$.

Figures 9 and 10 show the dimensionless groups for the velocity and temperature respectively. The present measurements are supplemented by a collection of previously published results from conventional grids with a secondary contraction [1-3, 11] and without a contraction [1-3, 9, 10]. For the data points obtained from reference [1-3, 9], the Taylor microscale Reynolds numbers are in the same range as those reported for the present measurements, i.e. $R_\lambda \sim 30 \rightarrow 50$. For reference [10], the measurements are obtained for at a much higher Reynolds number of $R_\lambda \sim 670$; for [11], $R_\lambda \sim 75$. With regard to the quality of the collapse in these figures, note that the influence of initial conditions, as felt through the large scales via $<q^2>$, tends to affect (31) and (32) more than (28)-(30). For clarity, we have only plotted in Figures 9 and 10 the curves for $r_* = 1.0$, $\alpha_u = 0.03$ and $n_u = n_\theta = -1.20$; these curves should serve as a visual guide for grid turbulence in general. Note that the empirical coefficients are expected to change with the initial conditions. For example, as reported in literature, depending on the geometry of the grid, n_u may vary from near -1 to -1.5 [e.g. 1-3, 5, 6, 9-11]. Also note that different methods of heating may affect the ratio n_u/n_θ [e.g. 8]. Nonetheless, the curves in Figures 9 and 10 demonstrate that the data points can be closely represented by the empirical relations. If required, design charts (not shown here) may be obtained by plotting (28)-(32) for specific values of $(t-t_o)U_o/M$ and R_M for particular grids or initial conditions. However, Figures 9 and 10 should be sufficient for providing reliable information on the basic flow parameters, at least for a particular grid geometry and selected values of M and R_M, prior to carrying out an experiment in a wind tunnel.

CONCLUDING REMARKS

From dimensional analysis we have obtained correlations between basic flow parameters in slightly heated, decaying grid turbulence. The correlations are in the form of empirical power laws which are exhibited by the trends for the (mean dissipation rates of) turbulence energy and scalar variance in the self-similar region of flow downstream of the grid. The empirical relations, i.e. (28)-(32), are supported by the present velocity and scalar (i.e. thermal) measurements for three different grid flows at small Reynolds and Péclet numbers as well as previously published data for grid turbulence at large Reynolds numbers. Perhaps the most significant observation here is that the relations involving the Kolmogorov scale (η), the Reynolds number (R_λ) and the Péclet number (Pe), as given by (28), (31) and (32) respectively, depend on the empirical (decay) exponent n_u for the grid. By observing a power-law rate of decay, it naturally follows from definitions (8) and (9) that the empirical relations involving the Taylor microscale λ (29) and the Corrsin microscale λ_θ (30), are "$1/2$" power-law functions of streamwise distance from the grid, i.e. $\left[\left(t-t_o\right)U_o/M\right]^{1/2}$. As a point of illustration, we have selected for (28)-(32) curves with the empirical coefficients $r_* = 1.0$, $\alpha_u = 0.03$ and $n_u = n_\theta = -1.20$ to serve as a visual guide to the trend of all the data points shown in Figures 8 and 9. In practice, however, it is preferable that the values of r_*, α_u, n_u and n_θ should be accurately determined for a particular grid of size M and selected values of mesh Reynolds number (R_M) before attempting to extract further information on the basic flow parameters (i.e. η, λ, λ_θ, R_λ and Pe).

ACKNOWLEDGMENTS

The authors gratefully acknowledge the financial support by the Australian Research Council.

REFERENCES

[1] Comte-Bellot, G., and Corrsin, S. (1966). The use of a contraction to improve the isotropy of grid-generated turbulence. *J. Fluid Mech.*, 25(4):657-682.

[2] Lavoie, P. (2006). *Effects of initial conditions on decaying grid turbulence*. Ph. D. Thesis, The University of Newcastle, Australia.

[3] Lavoie, P., Djenidi, L., and Antonia, R.A. (2007). Effects of initial conditions in decaying turbulence generated by passive grids. *J. Fluid Mech.*, 585:395-420.

[4] Antonia, R.A., Lavoie, P., Djenidi, L., and Benaissa, A. (2010). Effect of a small axisymmetric contraction on grid turbulence. *Exp. Fluids*, 49:3-10.

[5] Mohamed, M. S., and LaRue, J. C. (1990). The decay power law in grid-generated turbulence. *J. Fluid Mech.*, 219:195–214.

[6] Antonia, R.A., Smalley, R.J., Zhou, T., Anselmet, F., and Danaila, L. (2004). Similarity solution of temperature structure functions in decaying homogeneous isotropic turbulence. *Phys. Rev. E*, 69:016305.

[7] George, W. K. (1992). Self-preservation of temperature fluctuations in isotropic turbulence. In *Studies in turbulence*, pages 514–528, Springer-Verlag, New York.

[8] Sreenivasan, K. R., Tavoularis, S., Henry, R., and Corrsin, S. (1980). Temperature fluctuations and scales in grid-generated turbulence. *J. Fluid Mech.*, 100(3):597–621.

[9] Zhou, T., Antonia, R.A., Danaila, L., and Anselmet, F. (2000). Transport equations for the mean energy and temperature dissipation rates in grid turbulence. *Exp. Fluids*, 28:143-151.

[10] Kistler, A. L., and Vrebalovich, T. (1966). Grid turbulence at large Reynolds numbers. *J. Fluid Mech.*, 26(1):37–47.

[11] Krogstad, P. Å., and Davidson, P. A. (2010). Is grid turbulence Saffman turbulence? *J. Fluid Mech.*, 642:373–394.

[12] Corrsin, S. (1951). The dacay of isotropic temperature fluctuations in an isotropic turbulence. *J. Aeronaut. Sci.*, 18(6):417-423.

[13] Monin, A. S., and Yaglom, A. M. (1975). *Statistical Fluid Mechanics: Mechanics of Turbulence Volume 2*. The MIT Press, Cambridge.

[14] Batchelor, G. K. (1953). *The theory of homogeneous turbulence*. Cambridge University Press, Cambridge.

[15] Uberoi, M. S. (1956). Effect of wind-tunnel contraction on free-stream turbulence. *J. Aeronaut. Sci.*, 23(8):754–764.

[16] Antonia, R.A., Browne, L.W.B., and Chambers, A.J. (1981). Determination of time constants of cold wires. *Rev. Sci. Instrum.*, 52(9):1382-1385.